STUDY OF DEFORMATION BEHAVIOR OF AISI 1025 CARBON STEEL WITH DIFFERENT MICROSTRUCTURES USING METAL MAGNETIC MEMORY AND ACOUSTIC EMISSION TESTING
ДОСЛІДЖЕННЯ ДЕФОРМАЦІЙНОЇ ПОВЕДІНКИ ВУГЛЕЦЕВОЇ СТАЛІ AISI 1025 З РІЗНОЮ МІКРОСТРУКТУРОЮ З ВИКОРИСТАННЯМ МЕТОДІВ МАГНІТНОЇ ПАМ'ЯТІ МЕТАЛУ ТА АКУСТИЧНОЇ ЕМІСІЇ

by W. Sharatchandra Singh* and C.K. Mukhopadhyay†

* Non Destructive Evaluation Division (NDED), Indira Gandhi Centre for Atomic Research (IGCAR), Kalpakkam 603102, Tamil Nadu, India

† Formerly with NDED, IGCAR, Kalpakkam 603102, Tamil Nadu, India.

E-mail:ckm602003@gmail.com

Studies are carried out to investigate the tensile deformation behavior of AISI-type 1025 carbon steel with different microstructures using metal magnetic memory and acoustic emission testing (AE) techniques. Seven AISI 1025 carbon steel specimens were heat treated for different microstructures and then subjected to tensile deformation until fracture. AE was conducted during tensile deformation and the deformation- induced self-magnetic leakage fields (SMLFs) were measured using a giant magneto-resistive sensor after unloading. Results reveal that SMLF signal values are influenced by microstructure and residual stress aroused due to plastic deformation. Among different specimens, SMLF signal peak amplitude is highest in the brine-quenched specimen followed by the tempered specimen, while hardness is highest in the brine-quenched specimen. SMLF signal peak amplitude and hardness are the lowest in the annealed specimen. SMLF signal is higher in tempered specimens compared to the untempered specimens. From AE measurements, it is observed that martensitic steel emits higher acoustic emissions during deformation but decreases when tempered. The acoustic emissions generated in the martensitic steel are also of higher amplitude. The results are correlated with optical micrographs and hardness measurements.

Проведено дослідження з вивчення деформації розтягу вуглецевої сталі AISI типу 1025 з різною мікроструктурою з використанням методів магнітної пам'яті металу та акустичної емісії (AE). Сім зразків з вуглецевої сталі AISI 1025 було термічно оброблено для отримання різних мікроструктур, а потім піддано деформації розтягу до руйнування. AE проводили під час деформації розтягу, а викликані деформацією власні магнітні поля витоку (SMLF) вимірювали за допомогою датчика на основі гігантської магніторезистивної технології (GMR) після розвантаження. Результати показують, що на значення сигналу SMLF впливають мікроструктура та залишкове напруження, що виникає внаслідок пластичної деформації. Серед різних зразків пік амплітуди сигналу SMLF є найвищим у зразку, що загартований в соляному розчині, наступним за яким є зразок з відпуском, тоді як твердість є найвищою у зразку, загартованому в соляному розчині. Пікова амплітуда сигналу SMLF і твердість є найнижчими у відпаленому зразку. Вимірювання AE показали, що мартенситна сталь випромінює більшу акустичну емісію під час деформації, але зменшується під час відпуску. Акустична емісія, що виникає в мартенситній сталі, також має вищу амплітуду. Результати корелюють з оптичними мікрофотографіями та вимірюваннями твердості.

Keywords: metal magnetic memory, acoustic emission, microstructure, carbon steel, tensile deformation

Ключові слова: магнітна пам'ять металу, акустична емісія, мікроструктура, вуглецева сталь, деформація розтягу

Introduction

Ferromagnetic materials are widely used in metallic structures such as boilers, pipelines, and railway tracks. Among ferromagnetic materials, carbon steel is commonly used in view of its low cost and good mechanical properties (Vivekananda and Venkataraman 2006; Tang et al. 2019). These structures are constantly subjected to mechanical actions during service that can induce stress, leading to the development of cracks or even fractures that cause severe damage (Bao et al. 2015). Therefore, ongoing nondestructive evaluation (NDE) of the mechanical properties of these structures is of great importance for evaluating the state of structures in service before catastrophic failure.

Various NDE methods and techniques, such as ultrasonic testing, acoustic emission testing (AE), magnetic Barkhausen noise, and metal magnetic memory (MMM), have been used to evaluate the mechanical properties of ferromagnetic materials (Byeon and Kwun 2003; Song-ling et al. 2004). Among these, the MMM technique has gained considerable interest among nondestructive testing (NDT) researchers, because of its potential for the evaluation of early damage, micro-defects, and the stress state in ferromagnetic materials (Leng et al. 2013; Min et al. 2014; Xing et

al. 2006). This technique is found to be used in various NDT applications for diagnosing oil and gas pipelines, rails, turbine wheels, pressure vessels, and the like (Wang et al. 2012; Doubov 2001). The MMM technique relies on the measurement of the self-magnetic leakage field (SMLF) of ferromagnetic materials under the combined operation of external load and ambient geomagnetic field. In this technique, the distribution of SMLF induced at the stress-concentration zone (SCZ) during mechanical loading is measured using magnetic field sensors (Doubov 2001).

There are many factors affecting the strength of the SMLF signal such as the environmental magnetic field, stress distribution, and nature of material (Hu et al. 2010; Moonesan and Kashefi 2018; Bao and Zhang 2015; Sonntag et al. 2014; Singh et al. 2016). Moonesan and Kashefi (2018) studied the effect of sample initial magnetic field on SMLF signals and reported that SMLF signals exhibit a drop at the SCZ when the sample has a high level of initial residual magnetic field. Bao and Zhang (2015) analyzed the effect of loading speed on SMLF signals of C45 and Q235 ferromagnetic steels subjected to tensile stress. They observed that the variations of SMLF signals due to different loading speeds change systematically as the applied load increases. Sonntag et al. (2014) studied the change in the surface topography of a notched structural steel (S235JR) specimen due to tensile deformation using an optical 3D surface interferometer and its deformation-induced SMLFs using giant magneto-resistive (GMR) sensors. They reported that the measured SMLF is the result of the combined effect of stress and topography changes due to plastic deformation, and their separation is difficult to perform experimentally. Singh et al. (2016) studied the effect of geometry changes on SMLF signals in notched steel specimens during tensile deformation using finite element modeling. Their results indicated that the stress-induced geometry has a great influence on SMLF signals of about 20%, especially in the plastic deformation stage. Other studies (Liu et al. 2019; Long et al. 2014) also reported on the influence of microstructure on SMLF signals. Liu et al. (2019) discussed the grain size effect on SMLF signals for stress damage evaluation of low-carbon steel and concluded that the slope of the SMLF gradient decreases slightly as the grain size increases. Long et al. (2014) showed the potential of the MMM technique for revealing the tempering effect due to tensile deformation in C45 steel. However, information on the influence of microstructure on SMLF signals for heat-treated carbon steel is scarce in the literature.

On the other hand, acoustic emission is defined as the class of phenomenon whereby transient elastic waves are generated by the rapid release of energy from localized sources in a material (ASNT 2005). Wadley and Scruby (1991) investigated the acoustic emissions generated during tensile deformation of low-alloy steels with carbon content varying between 0.06 and 0.49 wt% and as a function of cooling rate. It was reported that specimens with (a) slowly cooled microstructures (with ≥10 μm ferrite dimension), (b) low initial dislocation density, and (c) very widely spaced precipitates, generate the highest acoustic emission activity. This was attributed to higher glide distance and higher velocity of dislocations in the ferrite phase (Wadley and Scruby 1991). Carpenter and Pfleiderer (1994) reported that the magnitude of root mean square (RMS) peak voltage at the yield stress region increases with increasing yield strength in AISI 4340 steel, tempered at different conditions. This was attributed to the increase in difficulty in initiating and propagating Lüders bands with increasing strength level (Carpenter and Pfleiderer 1994). Khamedi et al. (2010) studied the effect of the volume fraction of martensite on AE behavior of dual-phase steel (DPS) under tensile loading. AE dominant frequency was used to find different failure modes such as ferrite–martensite interface decohesion or martensite phase fracture. Haneef et al. (2010) studied the effect of heat treatment on Lüders band formation in medium carbon steel using AE. The decrease in acoustic emission activity in tempered specimens compared to water-quenched specimens was observed due to the decrease in dislocation activity. Monitoring of the deformation and fracture process of ferritic–martensitic DPS by employing AE was carried out by Fallahi et al. (2012). The DPS had different volume fractions of martensite (12%–73%) and various morphologies like equiaxed or fibrous martensite phase produced from low-carbon steel (0.1% C). The results show the usefulness of AE to detect failure micromechanisms consisting of ferrite–martensite interface decohesion and/or martensite phase fracture, and identifying the correlation of failure mechanisms to microstructure in DPS (Fallahi et al. 2012).

This paper presents studies carried out to investigate the tensile deformation behavior of AISI-type 1025 carbon steel with different microstructures using MMM and AE techniques. The effect of tempering on SMLF signals was studied. AE measurements were carried out during tensile deformation, while SMLF was measured after unloading the specimens. The results are correlated with optical micrographs and hardness measurements.

The next section of this paper presents the details of the material and tensile specimen including different heat treatment and corresponding microstructures. Next, the experimental setup of MMM and AE testing is described. The experimental results of tensile, MMM, and AE for different heat-treated specimens are presented

and discussed in the results and discussion section. Lastly, the conclusions drawn from the study are given.

Material and Heat Treatment

The material used in this study is an AISI-type 1025 carbon steel whose chemical composition (wt%) is given in Table 1. The tensile specimens (length of 200 mm, width of 20 mm, and thickness of 4 mm) were fabricated from the sheet material according to the specification given in the ASTM standard (2009). The dimensions of the specimens are shown in Figure 1.

The specimens were given different heat treatments (as per Table 2) to modify the microstructure and, hence, tensile properties. The microstructure of different specimens is shown in Figure 2, with a 500× microscope amplification. The microstructure of the untreated specimen contains medium-size grains of ferrite (white region) as a major constituent and a small amount of pearlite (black region in Figure 2a). The microstructure of the normalized specimen contains ferrite, pearlite, and a small amount of martensite (Figure 2b). The microstructure of the annealed specimen shows coarse grains of ferrite as a major constituent and a small amount of pearlite(-Figure 2c). During annealing, the specimen undergoes a slow cooling, resulting in coarse grains. The microstructure of the brine-quenched specimen is mostly martensitic and some retained austenite (Figure 2d). The brine-quenched and tempered specimen has a more refined and homogeneous microstructure with martensite as a major constituent (Figure 2e). The microstructure of the oil-quenched specimen shows martensite as a major constituent and a small amount of retained austenite (Figure 2f). The microstructure of the oil-quenched and tempered specimen has a more refined and homogeneous microstructure with martensite as a major con- stituent and a small amount of retained austenite (Figure 2g).

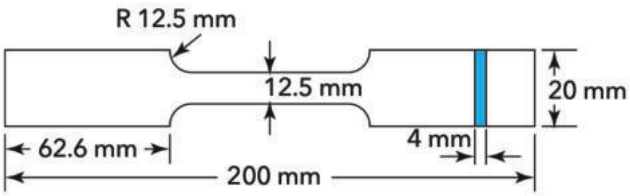

Figure 1. Dimensions of the tensile test specimen
Рис. 1. Розміри зразка для випробувань на розтяг

After the heat treatment, the specimens were ground and polished to remove any rust or dirt left on the surface. Tensile tests of all the specimens were carried out using a standard tensile testing machine with a crosshead speed of 1 mm/min at ambient temperature. The specimens were subjected to tensile deformation until fracture. A photograph of the fractured specimens is shown in Figure 3a. AE measurements were carried out during tensile deformation while the deformation-induced SMLFs were measured using a GMR sensor along the dotted line AB (shown in Figure 3b) after unloading and dismounting the specimens from the tensile testing machine.

Experimental Setup

In this section, the experimental setup of MMM and AE testing is described.

MMM Testing Setup

The experimental setup for MMM testing is shown in Figure 4. It consists of an in-house developed servo motor–based XY scanning system, GMR sensor tensile specimen, and computer. The scanning system consists of a servo motor and encoders to ensure smooth scanning with the position and speed feedback. The specimens were scanned with a GMR sensor along their centerline for detection of the tangential component of the SMLF from the fractured specimens. The scan step size and scanning speed were set to 10 μm and 20 mm/s, respectively. To avoid physical damage to the sensor, a liftoff

Table 1. Chemical composition (wt%) of AISI 1025 carbon steel used in study
Таблиця 1. Хімічний склад (мас.%) вуглецевої сталі AISI 1025, використаної в дослідженні

Element	C	Si	Mn	P	S	Cr	Ni	Al	Co	Cu	Nb	Ti	V	W	Fe
wt%	0.208	0.159	0.77	0.007	0.015	0.06	0.01	0.038	0.003	0.013	<0.003	0.002	<0.002	0.050	Bal.

Table 2. Details of heat treatment of AISI 1025 carbon steel tensile specimen
Таблиця 2. Дані термічної обробки зразка на розтяг з вуглецевої сталі AISI 1025

Specimen number	Heat treatment	Temperature (°C)	Hold time (min)	Quenching medium	Microstructure	Ranges of peak amplitude (dB)
S1	Untreated	–	–	–	Ferrite + pearlite	40–62
S2	Normalized	910	60	Air cooling	Ferrite + pearlite + martensite	40–68
S3	Annealed	910	60	Furnace cooling	Ferrite + pearlite	40–74
S4	Brine quenched	910	60	25% brine solution	Martensite + austenite	40–82
S5	Brine quenched and tempered	910 400	60 120	25% brine solution, furnace cooling	Martensite + austenite	40–82
S6	Oil quenched	910	60	Engine oil	Martensite + austenite	40–76
S7	Oil quenched and tempered	910 400	60 120	Engine oil, furnace cooling	Martensite + austenite	40–72

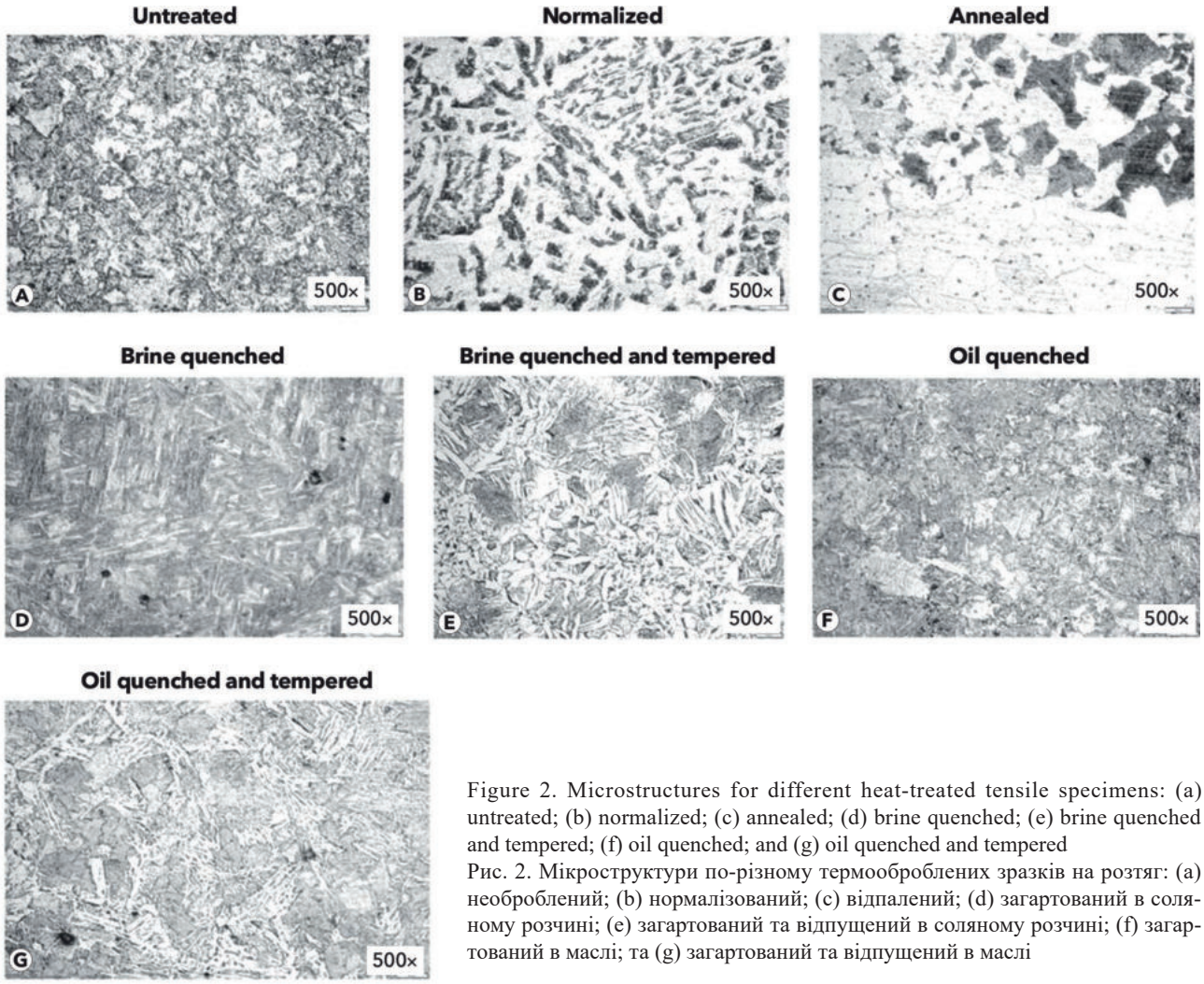

Figure 2. Microstructures for different heat-treated tensile specimens: (a) untreated; (b) normalized; (c) annealed; (d) brine quenched; (e) brine quenched and tempered; (f) oil quenched; and (g) oil quenched and tempered

Рис. 2. Мікроструктури по-різному термооброблених зразків на розтяг: (a) необроблений; (b) нормалізований; (c) відпалений; (d) загартований в соляному розчині; (e) загартований та відпущений в соляному розчині; (f) загартований в маслі; та (g) загартований та відпущений в маслі

of 1 mm was maintained between the GMR sensor and specimen surface. The GMR sensor output data was preamplified and then acquired through an analog-to-digital converter (ADC) card of 16-bit resolution and sampling frequency of 3.5 MS/s. The data was stored in a computer in a spreadsheet for subsequent analysis after voltage to magnetic field conversion (GMR output of 1 V corresponds to 3061 A/m). Data acquisition and signal visualization were performed using an in-house developed software.

AE Setup

The experimental setup used for AE measurement is shown in Figure 5. It consists of a 16-channel AE measurement system along with a broadband AE sensor with a frequency range of 100 kHz to 1 MHz and a resonant AE sensor with a frequency of 150 kHz. The sensor was attached firmly to the surface of each specimen by an elastic cord and a thin film of silicone grease for good transmittance of acoustic signals. The sensor was fixed at the gauge-to-shoulder transition region of the specimens. The AE data was recorded at a sampling rate of 5 MS/s for all the specimens. A preamplifier (40 dB gain) and bandpass filter (100 to 300 kHz) were used to record the

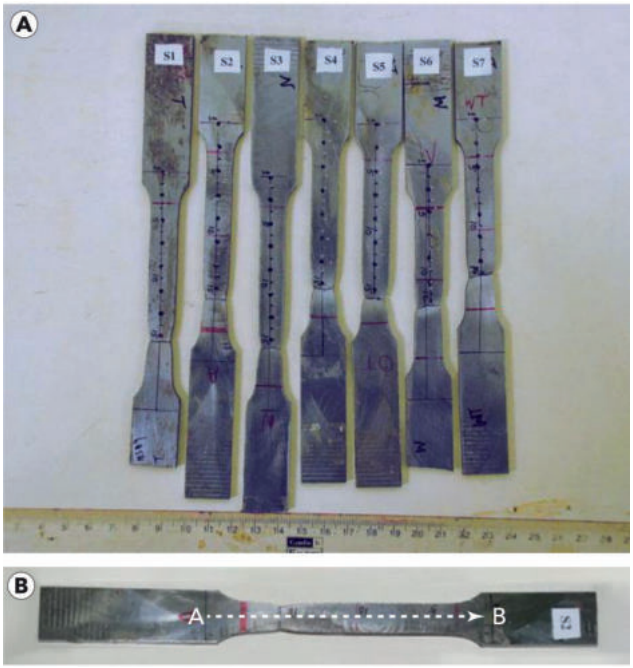

Figure 3. Fracture specimens: (a) photograph; (b) measurement of SMLF along the dotted line AB using a GMR sensor

Рис. 3. Зразки для випробувань на руйнування: (a) фотографія; (b) вимірювання SMLF уздовж пунктирної лінії AB за допомогою GMR датчика

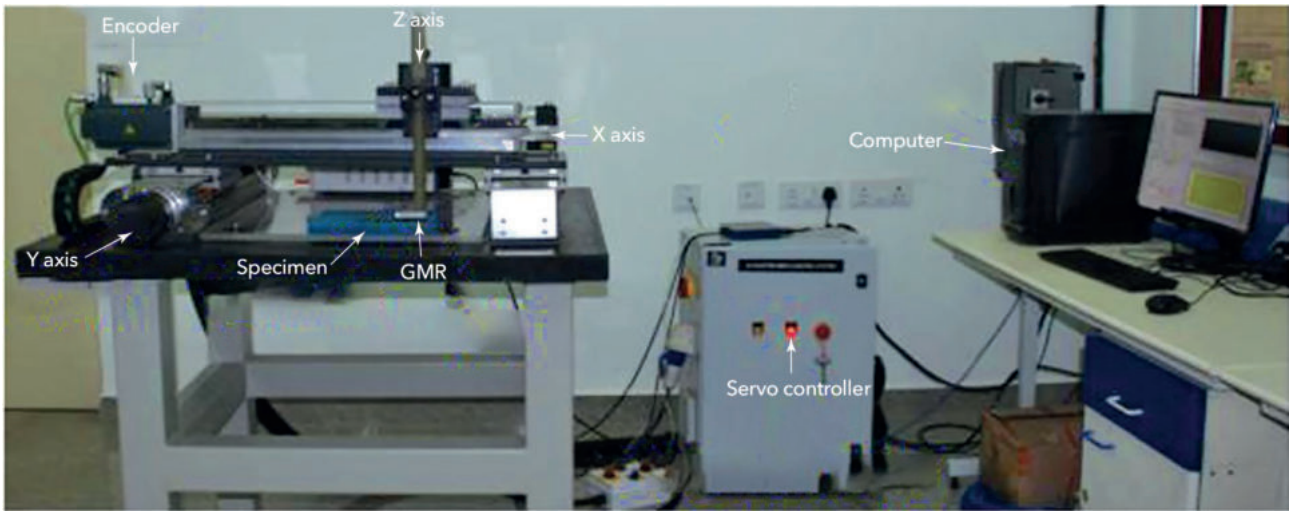

Figure 4. Experimental setup for MMM testing
Рис. 4. Експериментальна установка для досліджень магнітної пам'яті металу (MMM)

signals. A threshold of 40 dB was maintained. The gain and threshold were selected to mitigate external noise during recording.

This was done by repeatedly loading and unloading a dummy specimen to higher load levels expected to be taken by any of the specimens. This ensured that the acoustic emission signals were not recorded either from the machine or from external noise.

Results and Discussion

This section presents the results of the experiments.

Tensile Results

Stress-strain curves for all the specimens were generated from load-elongation plots and then tensile properties were determined. Figures 6a and 6b show the mechanical strengths (yield strength and tensile strength) and elongation, respectively, for the different heat-treated specimens. As can be seen from Figure 6a, both yield strength and tensile strength are highest for the brine-quenched specimen and lowest for the annealed specimen. The maximum strength in the brine-quenched specimen is primarily attributed to the presence of martensite as a major constituent, which is a very strong phase in carbon steels (Long et al. 2014; Adebiyi et al. 2015). The minimum strength in the annealed specimen is essentially due to relieving stress and an increase in grain size leading to free movement of dislocations. During annealing, the specimen undergoes slow cooling, which results in the formation of coarse grains and enhancement of ductility. The strength of the normalized specimen is found to be more than that of the annealed specimen due to the presence of a small amount of martensite in the normalized specimen. The strength of the oil-quenched and tempered specimen is reduced compared to the brine-quenched specimen. The effect of tempering on mechanical strength is more pronounced in the brine- quenched specimen compared to the oil-quenched specimen. This is attributed to the large difference in cooling rate for brine quenched and brine quenched followed by tempering compared to that of oil quenched and oil quenched followed by tempering.

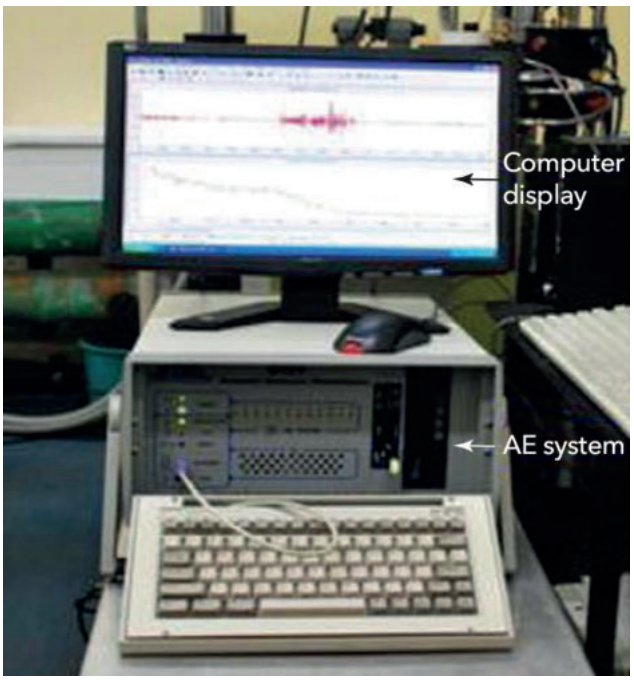

Figure 5. Experimental setup for AE
Рис. 5. Експериментальна установка для досліджень з використанням акустичної емісії (AE)

Among all the specimens, the annealed specimen shows maximum elongation while the brine-quenched specimen shows minimum elongation (Figure 6b). The maximum elongation in the annealed specimen is again attributed to the free movement of dislocations without any obstruction. The minimum elongation in the brine-quenched specimen is attributed to the presence of martensite. The brine quenching increases strength and reduces ductility. Tempering reduces strength but improves ductility of the steel.

The changes in tensile properties are influenced mainly by phase transition and residual stress. The

amounts of marten- site and ferrite are also important factors affecting tensile properties. The tempering process leads to changes in the internal structure of the steel and results in mechanical property changes.

MMM Results

Figure 7a shows the response of the GMR sensor for different specimens scanned along the full gauge length (measured length of 100 mm). As can be seen, the GMR sensor output (after voltage to magnetic field conversion) is different for different specimens, which implies that the SMLF depends upon the microstructure due to different heat treatments. This observation is attributed to the changes in the magnetic properties of carbon steel with the combined effect of microstructure and residual stress (because of tensile deformation) of the steel. As expected, the GMR sensor output is highest at the fracture position for all the specimens due to high magnetic reluctance at the fracture position (Bao et al. 2015). It is also observed that the peak position (~18 to 35 mm) is different for different specimens as the specimens were not fractured at the same location of gauge length.

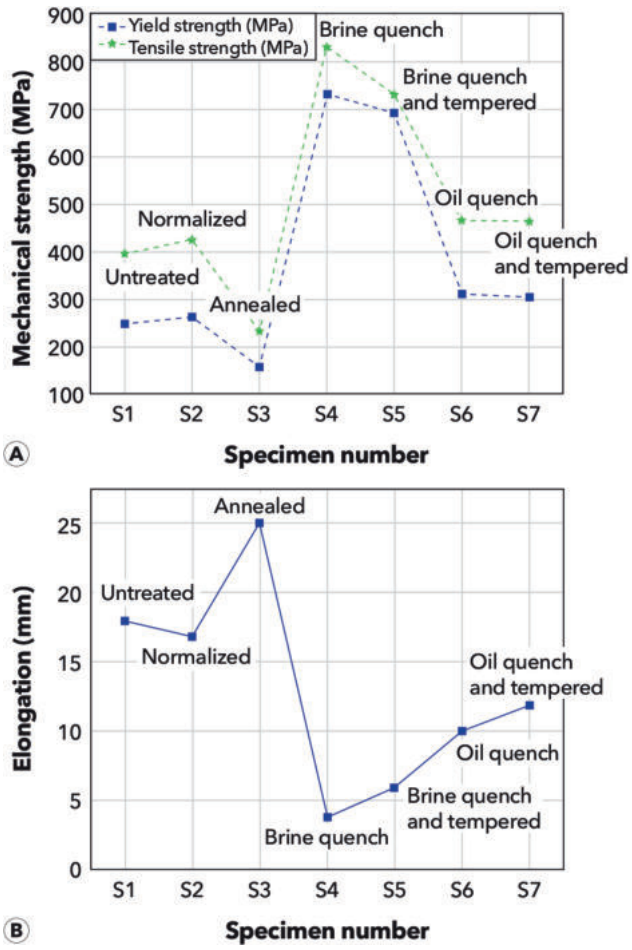

Figure 6. Comparison of different heat-treated specimens: (a) mechanical strength (yield strength and tensile strength); (b) elongation

Рис. 6. Порівняння зразків з різною термічною обробкою: (а) механічна міцність (границя текучості та міцність на розтяг); (b) подовження

In order to analyze the effect of plastic deformation on the SMLFs for all the heat-treated specimens, the response of the GMR sensor scanned along the longer piece of the fractured specimen is plotted in Figure 7b. It can be seen that the GMR sensor output is different due to plastic deformation in different specimens. The GMR sensor output also varies with the degree of plastic deformation. The intensity of the GMR sensor output is found to increase with the increase in deformation. When the tensile load is applied, the stress and magnetic which hinders the motion of the domain wall. It is equivalent to having a reluctance, leading to the distortion of magnetic flow. Therefore, the detectable leakage magnetic field increases and the SMLF signal increases as well.

The response of the GMR sensor for the untreated specimen with and without tensile deformation is also plotted in Figure 7c. As can be seen, the GMR output of the undeformed specimen is a straight line, and it has an average value of about 20 A/m. As compared to the undeformed specimen, the GMR output of the deformed specimen shows a peak at the fracture position and its value is also higher at the plastic deformation region due to the development of dislocation structures.

Hardness measurements (Figure 8a) were carried out at discrete positions (5 mm spacing) of the longer piece of the fractured specimens using a digital Rockwell hardness tester. As can be seen, the hardness values are different (average hardness ~150 to 270 HV) for different heat-treated specimens as well as for different positions of the same tensile deformed specimen. Hardness is highest in the brine-quenched specimen and lowest in the annealed specimen, as expected. The peak amplitudes of the GMR sensor output and hardness values for all the specimens were determined and plotted in Figure 8b. It can be seen that the GMR peak amplitude is highest in the brine-quenched and tempered specimen and lowest in the annealed specimen. The maximum GMR peak amplitude in the brine-quenched and tempered specimen is primarily attributed to its more refined and homogeneous martensitic structure and stronger ferromagnetism of tempered martensite than that of the quenched martensite (Long et al. 2014). After tempering, SMLF increases as the relative permeability values become higher due to tempering. The minimum GMR peak amplitude in the annealed specimen is essentially due to relieving stress and an increase in grain size leading to free movement of dislocations.

AE Results

Figures 9a through 9g show stress versus time plots for different specimens. The variations of acoustic emission counts with time are also superimposed on the same plots. According to the stress-strain curve, the tensile process in the untreated, normalized, and annealed specimens can be divided

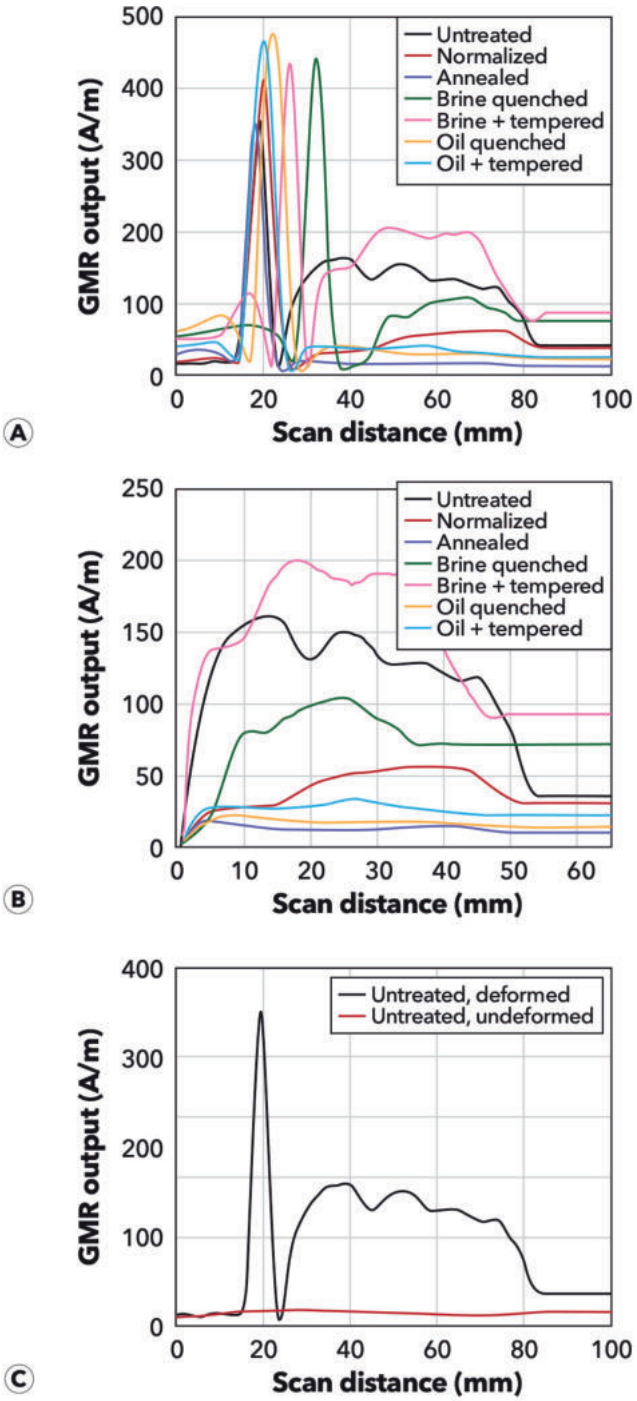

Figure 7. Response of GMR sensor for different heat-treated specimens: (a) scanned along the full gauge length; (b) scanned along longer piece of fractured specimen; (c) response of GMR sensor for the untreated specimen with and without tensile deformation (GMR output of 1 V corresponds to 3061 A/m)

Рис. 7. Відповідь датчика GMR для зразків з різною термічною обробкою: (a) сканування по всій ширині; (b) сканування уздовж довшого шматка зруйнованого зразка; (c) відповідь датчика GMR для необробленого зразка з деформацією розтягу та без неї (вихід GMR 1 В відповідає 3061 А/м)

into three regimes; namely, elastic region, Lüders or discontinuous yield region, and strain hardening region. In the brine-quenched, oil-quenched, and tempered specimens, the Lüders region is absent. In the quenched and tempered specimens, the presence of

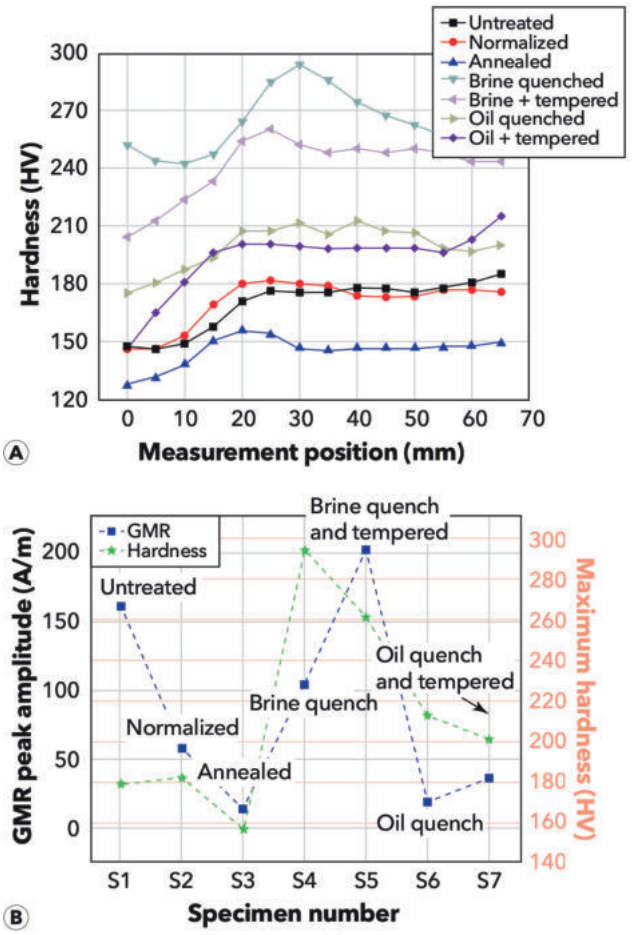

Figure 8. Comparison of different heat-treated specimens: (a) hardness measured at discrete positions of longer fractured specimen; (b) comparison of GMR peak signal amplitude with maximum hardness

Рис. 8. Порівняння зразків з різною термічною обробкою: (a) твердість, виміряна в дискретних положеннях довшого зруйнованого зразка; (b) порівняння амплітуди пікового сигналу GMR з максимальною твердістю

martensite causes initial yielding to commence at low stresses and the stress-strain curve becomes smooth and rounded. This is due to the presence of large densities of new dislocations created by martensitic transformation; retained austenite, which is much softer; and residual stresses after quenching, which assist in local yielding at low applied loads. Peak amplitude distribution of acoustic emission hits (or events) of two specimens (untreated and brine quenched) is shown in Figures 10a and 10b. Ranges of peak amplitude for different specimens are shown in Table 2.

In the untreated specimen (Figure 9a), higher counts are generated during preyield and yield deformation, and this is attributed to the generation and movement of dislocations. In the elastic region, emission is high. The acoustic emission counts in the Lüders region are comparatively lesser than the elastic region, and this is attributed to the reduced dislocation motion caused by an increase in dislocation density. At higher strain levels, a lesser num-

ber of counts compared to up-to-yield is due to the reduction in glide distance and velocity of moving dislocations. AE signals emitted by the normalized specimen are given in Figure 9b, where acoustic-emission activity is higher in the elastic and Lüders region in comparison with the strain-hardening region. Higher counts in the normalized specimen than in the case of the untreated specimen are due to the presence of martensite and the heterogeneous nature of the microstructure. In the case of the annealed specimen (Figure 9c), acoustic emission counts are significantly higher in the elastic region and reduced in the Lüders region and work-hardening region. Thus, in general, acoustic emission activity in untreated, normalized, and annealed specimens shows higher counts in the elastic region. In carbon steels, an increase in acoustic emission activity near yield point and a decrease thereafter was reported (Akbari and Ahmadi 2010). Acoustic emissions generated during micro-yielding were attributed to dislocation activity at grain boundaries and a rapid increase in acoustic emissions after massive plastic deformation was attributed to intensive development of slip bands in ferrite grains and Lüders band propagation in the lower yield point (Wang et al. 2015).

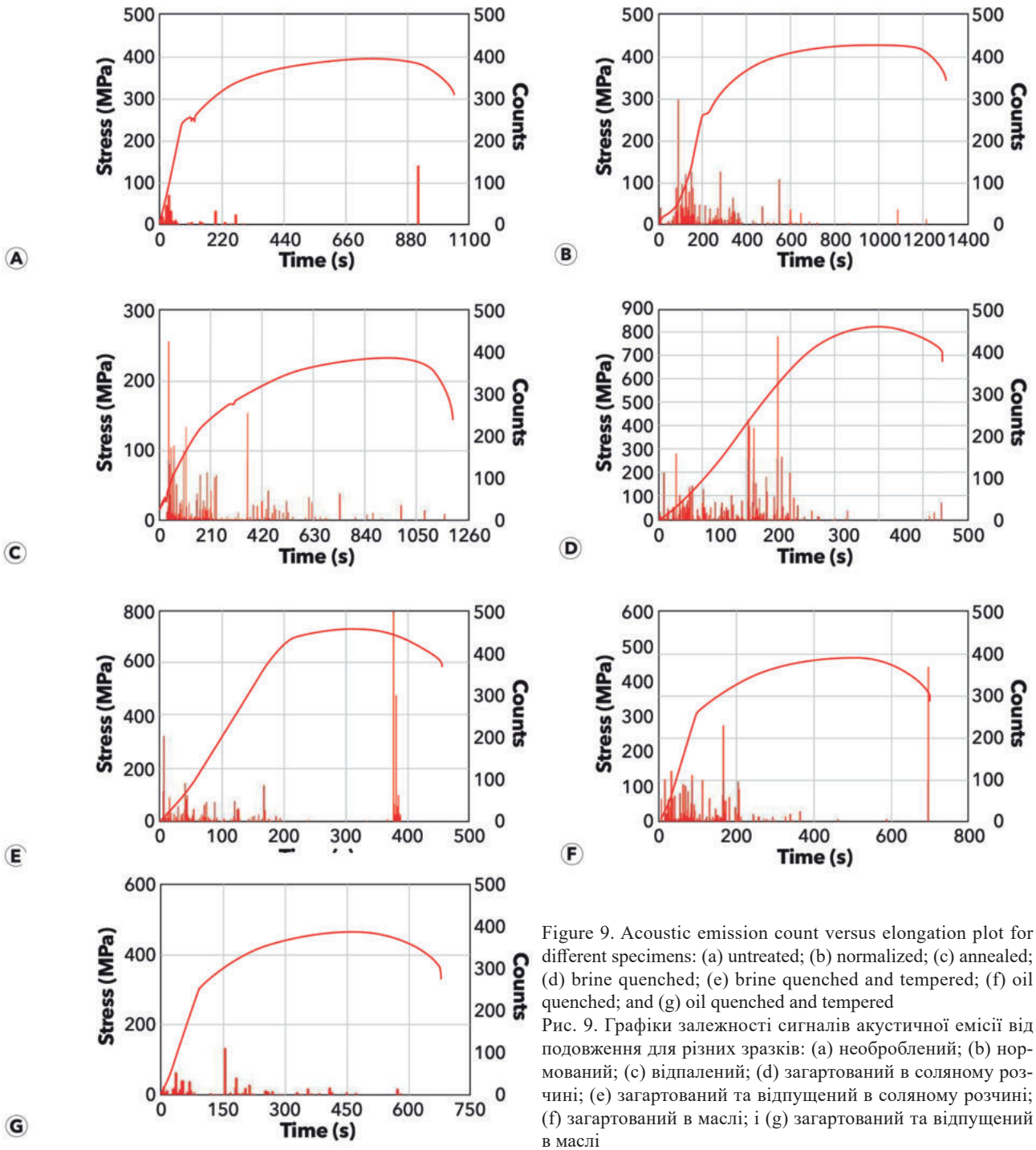

Figure 9. Acoustic emission count versus elongation plot for different specimens: (a) untreated; (b) normalized; (c) annealed; (d) brine quenched; (e) brine quenched and tempered; (f) oil quenched; and (g) oil quenched and tempered

Рис. 9. Графіки залежності сигналів акустичної емісії від подовження для різних зразків: (a) необроблений; (b) нормований; (c) відпалений; (d) загартований в соляному розчині; (e) загартований та відпущений в соляному розчині; (f) загартований в маслі; і (g) загартований та відпущений в маслі

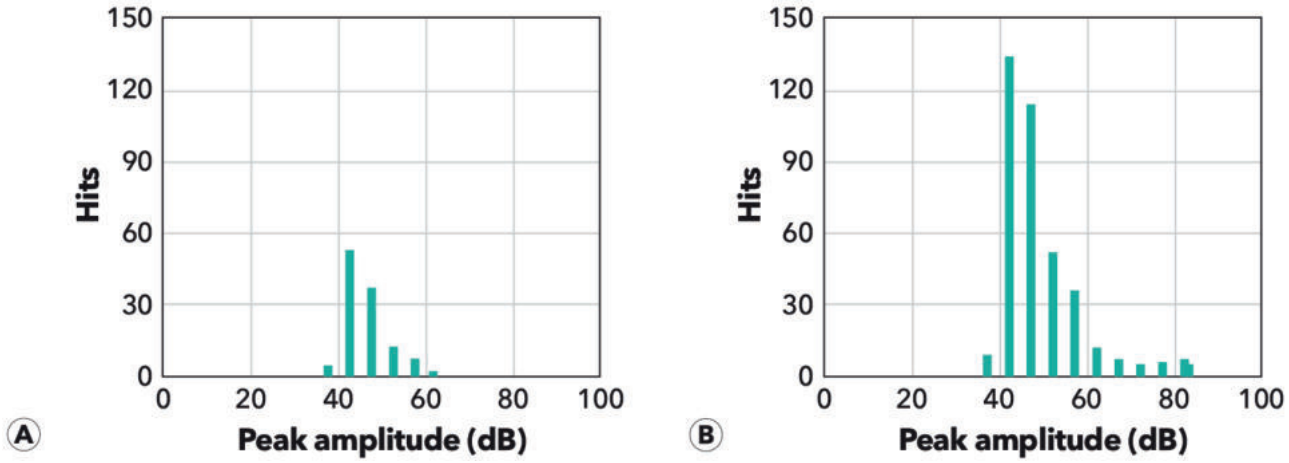

Figure 10. Distribution of acoustic emission hits by peak amplitude: (a) untreated; (b) brine quenched
Рис. 10. Розподіл сигналів акустичної емісії за піковою амплітудою: (а) необроблений; (b) загартований в соляному розчині

In the brine-quenched specimen (Figure 9d), acoustic emission counts are generated continuously from the beginning and are higher during strain hardening compared to the elastic region. The acoustic emission counts in the oil- quenched specimen (Figure 9f) follow an almost similar trend. The increasing acoustic emission activity with strain in quenched specimens could be attributed to cracking at interfaces and in martensitic particles. This generates signals of higher amplitude in these two specimens compared to the untreated, normalized, and annealed specimens (Table 2). The number of hits in the brine-quenched specimen is also higher compared to the untreated specimen (Figure 10). In DPS, for tensile fracture of samples with low martensite content, the dominant micromechanism of failure is ferrite/ martensite interface decohesion; but in samples with high martensite content, martensite phase fracture is also observed (Khamedi et al. 2010; Fallahi et al. 2012). The cracking in martensite is apparently related to the residual stress at the interfaces and the toughness of the martensitic particles them- selves (Long and Huazi 1990). After tempering, residual stresses are considerably reduced. This decreases acoustic emission counts in both of the tempered specimens (Figures 9e and 9g). A decrease in acoustic emissions in tempered specimens compared to quenched specimens is known (Haneef et al. 2010).

This study demonstrates that the SMLF is influenced by microstructure as well as residual stress aroused due to plastic deformation in heat-treated AISI 1025 carbon steel. Similar effects are found in acoustic emission signals and mechanical properties. AE is effective in evaluating the deformation behavior of heat-treated carbon steel specimens during tensile deformation, while the MMM technique is effective in evaluating deformation behavior after testing. Therefore, it is recommended to use both MMM and AE techniques for comprehensive understanding of deformation and, hence, damage estimation of carbon steel. The MMM technique is semivolumetric, which is sensitive to only surface and near-surface discontinuities and deformation. On the other hand, AE is a volumetric technique, which is sensitive to deformation and damage occurring throughout the volume of the material. Also, the MMM technique can be used only for ferromagnetic materials, while AE can be used for both ferromagnetic and nonferromagnetic materials. Further, it is suggested to consider the microstructure effect for reliable damage estimation of engineering components using the MMM technique. It will be beneficial to develop techniques to differentiate the effect of microstructure and residual stress in tensile-deformed carbon steels. Efforts are underway in this direction.

Conclusions

MMM and AE measurements were carried out to investigate the tensile deformation behavior of AISI 1025 carbon steel with different microstructures. The results show that SMLF signals are influenced by microstructure as well as residual stress in AISI 1025 carbon steels. Among various specimens, SMLF signal peak amplitude is highest in brine-quenched specimens followed by tempering, while hardness is highest in the brine-quenched specimen. However, SMLF signal peak amplitude and hardness are lowest in the annealed specimen. The SMLF signal is found to be more in tempered specimens compared to untempered specimens. From AE measurements, it is observed that AE in untreated, normalized, and annealed specimens shows higher counts in the elastic region. The quenched specimens with higher martensite emit higher acoustic emissions during deformation but decreases when tempered. Acoustic emissions in the quenched specimens generate a signal of higher amplitude than the tempered specimens. These results would be useful for reliable estimation of damage in engineered structures using MMM and AE techniques. They could also be used to provide effective feedback on the heat-treatment process.

Acknowledgments

Authors are thankful to Dr. Shaju K. Albert, Former Director, Metallurgy and Materials Group (MMG), IGCAR, and Dr. R. Divakar, Associate Director, Materials Characterization & Engineering Group, MMG, IGCAR, for encouragement and support.

References

1. Adebiyi, K.A., L.O. Mudasiru, and I.A. Babatunde, 2015, "Effect of Brine Solution on Grain Size Formations in AISI 1080 Low Carbon Steel," *IOSR Journal of Mechanical and Civil Engineering*, Vol. 12, No. 3, pp. 178–183, https://doi.org/10.9790/1684-1232178183
2. Akbari, M., and M. Ahmadi, 2010, "The Application of Acoustic Emission Technique to Plastic Deformation of Low Carbon Steel," *Physics Procedia*, Vol. 3, pp. 795–801, https://doi.org/10.1016/j.phpro.2010.01.102
3. ASNT, 2005, *Nondestructive Testing Handbook, Vol. 6: Acoustic Emission Testing*, 3rd edition, American Society for Nondestructive Testing, Columbus, OH
4. ASTM, 2009, ASTM E8/E8M: *Standard Test Methods for Tension Testing of Metallic Materials*, ASTM International, West Conshohocken, PA
5. Bao, S., and D. Zhang, 2015, "The Effect of Loading Speed on the Residual Magnetic Field of Ferromagnetic Steels Subjected to Tensile Stress," *Insight*, Vol. 57, No. 7, pp. 401–405, https://doi.org/10.1784/insi.2015.57.7.401
6. Bao, S., X. Liu, and D. Zhang, 2015, "Variation of Residual Magnetic Field of Defective U75V Steel Subjected to Tensile Stress," *Strain*, Vol. 51, pp. 370–378, https://doi.org/10.1111/str.12147
7. Byeon, J.W., and S.I. Kwun, 2003, "Magnetic Evaluation of Microstructures and Strength of Eutectoid Steel," *Materials Transactions*, Vol. 44, No. 10, pp. 2184–2190
8. Carpenter, S.H., and C. Pfleiderer, 1994, "Acoustic Emission from AISI 4340 Steel as a Function of Strength," *Journal of Acoustic Emission*, Vol. 12, pp. 141–148
9. Doubov, A.A., 2001, "Diagnostics of Equipment and Constructions Strength with Usage of Magnetic Memory," *Inspection Diagnostics*, Vol. 6, pp. 19–29
10. Fallahi, A., R. Khamedi, G. Minak, and A. Zucchelli, 2012, "Monitoring of the Deformation and Fracture Process of Dual Phase Steels Employing Acoustic Emission Techniques," *Materials Science and Engineering: A*, Vol. 548, pp. 183–188, https://doi.org/10.1016/j.msea.2012.03.104
11. Haneef, T.K., C.K. Mukhopadhyay, B.P.C. Rao, and T. Jayakumar, 2010, "Acoustic Emissions Generated during Lüders Band Elongation of Tempered Medium Carbon Steel," *Strength, Fracture and Complexity*, Vol. 6, pp. 149–159, https://doi.org/10.3233/SFC-2011-0113
12. Hu, B., L. Li, X. Chen, and L. Zhong, 2010, "Study on the Influencing Factors of Magnetic Memory Method," *International Journal of Applied Electromagnetics and Mechanics*, Vol. 33, pp. 1351–1357, https://doi. org/10.3233/JAE-2010-1260
13. Khamedi, R., A. Fallahi, and A.R. Oskouei, 2010, "Effect of Martensite Phase Volume Fraction on Acoustic Emission Signals Using Wavelet Packet Analysis during Tensile Loading of Dual Phase Steels," *Materials & Design*, Vol. 31, pp. 2752–2759, https://doi.org/10.1016/j.matdes.2010.01.019
14. Leng, J., Y. Liu, G. Zhou, and Y. Gao, 2013, "Metal Magnetic Memory Signal Response to Plastic Deformation of Low Carbon Steel," *NDT & E International*, Vol. 55, pp. 42–46, https://doi.org/10.1016/j.ndteint.2013.01.005
15. Liu, B., X. Xue, J. Li, R. Li, S. Dong, and J. Fang, 2019, "Grain Size Effect on Metal Magnetic Memory Signal for Stress Damage Evaluation of Low Carbon Steel," *Nondestructive Testing and Evaluation,* Vol. 34, No. 3, pp. 267–282, https://doi.org/10.1080/10589759.2019.1590830
16. Long, F., J. Wang, G. Gao, W. Li, and J. Zhao, 2014, "Tempering Effect and Tensile Properties Evaluation of C45 Steel Based on Magnetic Memory Technology," *Materials Evaluation*, Vol. 72, No. 11, pp. 1414–1420
17. Long, Q.Y., and Y. Huazi, 1990, "Acoustic Emission during Deformation of Dual-Phase Steels," *Metallurgical Transactions A*, Vol. 21, No. 1, pp. 373–379, https://doi.org/10.1007/BF02782417
18. Min, Y., G. Rui-Bin, Z. Chunyu, Q. Yinhu, S. Zhiyuan, and X. Zhanshan, 2014, "Research on the Relationship between Metal Magnetic Memory Signal Distortion and Yield Strain under Static Tension Test," *Insight*, Vol. 56, No. 12, pp. 669–675, https://doi.org/10.1784/insi.2014.56.12.669
19. Moonesan, M., and M. Kashefi, 2018, "Effect of Sample Initial Magnetic Field on the Metal Magnetic Memory NDT Result," *Journal of Magnetism and Magnetic Materials*, Vol. 460, pp. 285–291, https://doi.org/10.1016/j.jmmm.2018.04.006
20. Singh, W.S., R. Stegemann, and M. Kreutzbruck, 2016, "Three-Dimensional Finite Element Analysis of the Stress-Induced Geometry Effect on Self-Magnetic Leakage Fields during Tensile Deformation," *Insight*, Vol. 58, No. 10, pp. 544–550, https://doi.org/10.1784/insi.2016.58.10.544
21. Song-ling, H., L. Lu-ming, S. Ke-ren, and W. Xiao-fen, 2004, "Magnetic Field Properties caused by Stress Concentration," *Journal CSUT*, Vol. 11, No. 1, pp. 23–26
22. Sonntag, N., R. Stegemann, B. Skrotzki, and M. Kreutzbruck, 2014, "Deformation Induced Magnetization of Ferromagnetic Steels Using the Example of an Unalloyed Structural Steel," *Proceedings of the Werkstoffprüfung*, pp. 355–360 (in German)
23. Tang, J., J. Li, H. Wang, Y. Wang, and G. Chen, 2019, "In-Situ Monitoring and Analysis of the Pitting Corrosion of Carbon Steel by Acoustic Emission," *Applied Sciences*, Vol. 9, https://doi.org/10.3390/app9040706
24. Vivekananda, K.S., and K.S. Venkataraman, 2006, "NDE Techniques for Reliable Inspection of Carbon Steel Tubes," *Proceedings of National Seminar on Non-Destructive Evaluation*, 7–9 December, Hyderabad, India
25. Wadley, H.N.G., and C.B. Scruby, 1991, "Cooling Rate Effects on Acoustic Emission-Microstructure Relationships in Ferritic Steels," *Journal of Mate rials Science,* Vol. 26, pp. 5777–5792, https://doi.org/10.1007/BF01130115
26. Wang, H.W., H.M. Yu, H.Q. Xiao, Z.Y. Han, and H.Y. Luo, 2015, "Steel Damage based on Acoustic Emission," *Materials Research Innovations*, Vol. 19, https://doi.org/10.1179/1432891714Z.0000000001094
27. Wang, Z.D., Y. Gu, and Y.S. Wang, 2012, "A Review of Three Magnetic NDT Technologies," *Journal of Magnetism and Magnetic Materials*, Vol. 324, pp. 382–388, https://doi.org/10.1016/j.jmmm.2011.08.048
28. Xing, C., L. Luming, H. Bin, C. Xiaojie, D. Yuanhui, Y. Dezhi, and Y. En, 2006, "Magnetic Evaluation of Fatigue Damage in Train Axles without Artificial Excitation," *Insight*, Vol. 48, No. 6, pp. 342–345, https://doi. org/10.1784/insi.2006.48.6.342

Premission to Reprint 20.10.2022:
The American Society for Nondestructive Testing, Inc.
CITATION
Materials Evaluation 80 (6): 44-53
https://doi.org/10.32548/2022.me-04195